Supporting Information

Understanding MXene Based "Symmetric" Supercapacitors and Redox Electrolyte Energy Storage

Yapeng Tian[a], Chenhui Yang[a], Yangyang Luo[a], Hongyang Zhao[b],

Yaping Du*[,b] Ling Bing Kong*[,c], and Wenxiu Que*[,a]

[a] Electronic Materials Research Laboratory, International Center for Dielectric Research, Key Laboratory of the Ministry of Education, Shaanxi Engineering Research Center of Advanced Energy Materials and Devices, School of Electronic & Information Engineering, Xi'an Jiaotong University, Xi'an 710049, Shaanxi, People's Republic of China

[b] Frontier Institute of Science and Technology, Xi'an Jiaotong University, Xi'an 710049, Shaanxi, People's Republic of China

[c] College of New Materials and New Energies, Shezhen Technology University, Shenzhen 518118, Guangdong, People's Republic of China

Corresponding author: Prof. W. Que, Prof. Y. Du and Prof. L. B. Kong

E-mail address: wxque@mail.xjtu.edu.cn (W. Que), ypdu2013@mail.xjtu.edu.cn (Y. Du) and konglingbing@sztu.edu.cn (L. B. Kong).

List of content

investigate the real capacitance behavior of electrode materials in the positive and negative potential range, thus avoiding the interaction between the positive and negative electrodes.

Fig. S8 CV curves of the $Ti_3C_2T_x$ based symmetric SC for the first 3 cycles at different scan rates: (a) 5 mV s^{-1}, (c) 10 mV s^{-1}, (e) 20 mV s^{-1} and (g) 50 mV s^{-1}. CV curves of the $Ti_3C_2T_x$ based symmetric SC after activation at different scan rates: (b) 5 mV s^{-1}, (d) 10 mV s^{-1}, (f) 20 mV s^{-1}, and (h) 50 mV s^{-1}.

Fig. S9 The blue area is the available potential for Ti_3C_2 MXene in 3 M H_2SO_4 electrolyte; N and P represent the potential of the positive and negative electrodes, respectively.

Fig. S10 (a) Parameters: P_N and P_P represent the potential of the negative and positive electrodes, respectively. P_{0V} represents the potential of both electrodes when the SCs are operated at 0 V. **(b)** Illustration of P_{0V} shifting to a lower potential with electrochemical surface modification.

Fig. S11. (a) CV curves of the positive electrode at the scan rates of 2, 5, 10, 20 and 50 mV s^{-1}. (b) GCD curves of the positive electrode at different current densities. (c) CV curves of the negative electrode at the scan rates of 2, 5, 10, 20 and 50 mV s^{-1}. (d) GCD curves of the negative electrode at different current densities. All the data were tested under the condition of three-electrode system.

Fig. S12. In situ XRD patterns for the negative electrode (a) and positive electrode in the mixed electrolyte (b), the negative electrode (c) and the positive electrode (d) in the H_2SO_4 electrolyte. (e) The XRD patterns for the positive electrode for the sample of the activated electrode (after 30 cyclings) and the sample after 5000 cycles in the mixed electrolyte.

Fig. S13 (a) GCD curves for the cell in the mixed electrolyte at different current densities. (b) Gravimetric capacitance and volumetric capacitance of the cell in the mixed electrolyte calculated from the GCD curves. (c) GCD curves of the MXene

electrode in the mixed electrolyte at different current densities in the form of three-electrode system. (d) Gravimetric capacitance and volumetric capacitance of the MXene electrode in the mixed electrolyte in the form of three-electrode system calculated from the GCD curves.

Fig. S14 CV curves for the MXene electrode in 3 M H_2SO_4 + 0.2 M KI (a) and 1 M H_2SO_4 + 0.2 M KI (b) in the form of three-electrode system. (c) Volumetric capacitance of the electrode in different electrolytes at different scan rates calculated from the CV data. CV curves of the MXene based cells in 3 M H_2SO_4 + 0.2 M KI (d) and 1 M H_2SO_4 + 0.2 M KI (e) electrolytes. (f) Volumetric capacitance of the cell in different electrolytes at different scan rates calculated from the CV data. (g) Volumetric energy density of the cell in different electrolytes at different scan rates.

Fig. S15. CV curves of the MXene electrode with different real mass loading in 3 M H_2SO_4 + 0.2 M KI electrolyte under three-electrode system at the scan rates of 2, 5, 10, 20, and 50 mV s^{-1}: (a) 1.8, (b) 1.6 and (c) 1.2 mg cm^{-2}. (d) Volumetric capacitance of the MXene electrode with different real mass loadings at different scan rates.

Fig. S16. GCD curves of the $Ti_3C_2T_x$ film based SCs in 3 M H_2SO_4 (a) and 3 M H_2SO_4 + 0.2 M KI electrolytes (b). GCD curves of the $Ti_3C_2T_x$ film based SCs in 3 M H_2SO_4 and 3 M H_2SO_4 + 0.2 M KI electrolytes based on the total mass of the two electrodes at differnt current densities: (c) 1 A g^{-1}, (d) 5 A g^{-1} and (e) 50 A g^{-1}.

Fig. S17. (a) Nyquist plots of the $Ti_3C_2T_x$ film based cells in 3 M H_2SO_4 and 3 M H_2SO_4 + 0.2 M KI electrolytes and its electrical equivalent circuit. (b) Magnified high-frequency region of the Nyquist plots.

Calculation.

Gravimetric capacitance, C_g (F g^{-1}), of the working electrode can be calculated from the CV curves by using the following equation:

$$C_g = \int I \, dV / (2 \, m \, s \, \Delta V), \quad \text{(S1)}$$

where I (A) is the response current of the CV curve, s (V s^{-1}) is the scan rate, ΔV (V) is the potential window and m (g) is the mass loaded in working electrode.

Volumetric capacitance , C_v (F cm^{-3}), of the working electrode can be also calculated from the CV curves by using the following equation:

$$C_v = \int I \, dV / (2 \, V \, s \, \Delta V), \quad \text{(S2)}$$

where V (cm^3) is the volume of the film in working electrode.

Gravimetric capacitance, $C_{g,cell}$ (F g^{-1}), of the symmetric supercapacitors can be calculated from the CV curves by using the following equation:

$$C_{g,cell} = \int I \, dV / (2 \, m \, s \, \Delta V), \quad \text{(S3)}$$

where I (A) is the response current of the CV curves, s (V s^{-1}) is the scan rate, ΔV (V) is the potential window and m (g) is the total mass loaded in two electrodes.

Volumetric capacitance, $C_{v,cell}$ (F cm^{-3}), of the symmetric supercapacitors can be calculated from the CV curves by using the following equation:

$$C_{v,cell} = \int I \, dV / (2 \, V \, s \, \Delta V), \quad \text{(S4)}$$

where V (cm^3) is the total volume of the films in two electrodes.

Energy density, E (Wh L^{-1} or Wh kg^{-1}), and power density, P (W L^{-1} or W kg^{-1}), of the symmetric supercapacitors can be calculated according to the following equations:

$$E_g = \int V(t) \, I \, dt / M \quad \text{(S5)}$$

$$Ev = \int V(t) \, I \, dt / V \quad \text{(S6)}$$

$$P = 3600 \, E/\Delta t, \quad \text{(S7)}$$

where V(t) (V) is the discharge voltage excluding the IR drop, i is the current (A), M and V are total mass and volume of the active materials (cathode and anode), respectively.

Testing of the working potentials of the negative and positive electrodes *vs.* Hg/Hg_2SO_4 electrode

The working voltage ranges of the negative electrode were measured with the two-electrode configuration in 3 M H_2SO_4 at room temperature. A multimeter was connected to the negative electrode and the reference electrode (Hg/Hg_2SO_4 electrode) to mesure the potential of the negative electrode *vs.* the reference electrode, when the cyclic voltammetry was tested at different scan rates. Therefore, the potential of the positive electrode *vs.* the reference electrode can be obtained with the voltage between the positive electrode and the negative electrode is 1 V.

Materials

Unless otherwise indicated, all the chemicals (analytical grade) were from Shanghai Aladdin Biochemical Polytron Technologies Inc, China.

Synthesis of Ti_3AlC_2 powders

Firstly, the mixed powders of TiC (2-4 μm, 99%, Aladdin), Al (1-3 μm, 99.5%, Aladdin) and Ti (≤ 48 μm, 99.99%, Aladdin), with a molar ratio of 2:1.2:1, were ball-milled in absolute ethyl alcohol for 4 h at a speed of 350 rpm. Then, the mixture was sintered at 1400 °C for 2 h in Ar atmosphere. Finally, the sintered product was further ground to obtain fine powders, which were then sieved through a 400 mesh screen.

Materials characterization

Microstructure and elemental composition of the samples were characterized by using field-emission scanning electron microscopy (FE-SEM, Hitachi S-4800), equipped with energy-dispersive X-ray analysis (EDAX) (Hiroba). The morphological properties of the samples were observed by using transmission electron microscopy (TEM, FEI company Tecnai G220 S-twin, 200 kV). X-ray diffraction (XRD) patterns of the samples were recorded by using a Rigaku D/max 2200pc diffractometer, with Cu Kα radiation of wavelength λ= 0.15418 nm, at 40 kV and 40 mA. X-ray photoelectron spectroscopy (XPS) measurements of the samples were fulfilled by utilizing a Thermo Fisher ESCALAB Xi^+ with an exciting source of Al Kα.

Table S1 Working potential ranges for the positive and negative electrodes at different scan rates.

Scan rate ($mV\ s^{-1}$)	Potential range for the positive electrode (V vs. Hg/Hg_2SO_4)	Absolute potential for the positive electrode (V)	Potential range for the negative electrode (V vs. Hg/Hg_2SO_4)	Absolute potential for the negative electrode (V)
2	-0.702 ~ -0.108	0.594	-1.108 ~ -0.702	0.406
5	-0.715 ~ -0.105	0.61	-1.105 ~ -0.715	0.39
10	-0.720 ~ -0.100	0.62	-1.100 ~ -0.100	0.38
20	-0.720 ~ -0.080	0.64	-1.080 ~ -0.720	0.36
50	-0.720 ~ -0.070	0.65	-1.070 ~ -0.720	0.35

As shown in Table S1, the working potential ranges for the positive and negative electrodes show a unsettle from 2 to 50 $mV\ s^{-1}$, which were derived from the modified two-electrode systems in the H_2SO_4 electrolyte. As a result, this observation is not contradictory to the conclusion that the specific capacitance of the negative electrode is much higher than that of the positive electrode in the MXene based symmetric SCs. Therefore, the specific capacitances at 2, 5, 10, 20 and 50 $mV\ s^{-1}$ of the negative electrode are not in full agreement with the expected values, as those presented in Fig. 2f of the manuscript.

Table S2. The resistance for the cell in different electrolytes.

Resistance / Electrolyte	Rs (Ω cm^2)	Rct (Ω cm^2)
3 M H_2SO_4	0.50	1.0
3 M H_2SO_4 + 0.2 M KI	0.52	1.6

Fig. S1

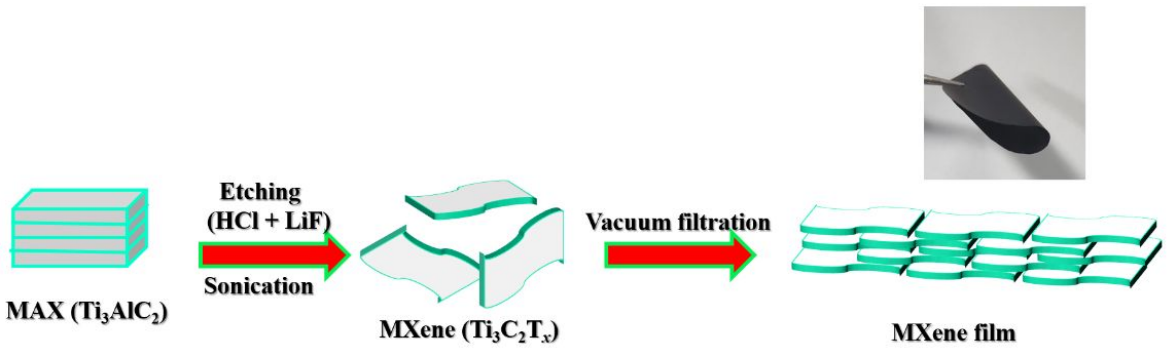

Fig. S1. Schematic diagram of preparation progress of the $Ti_3C_2T_x$ and flexible films.

Fig. S2

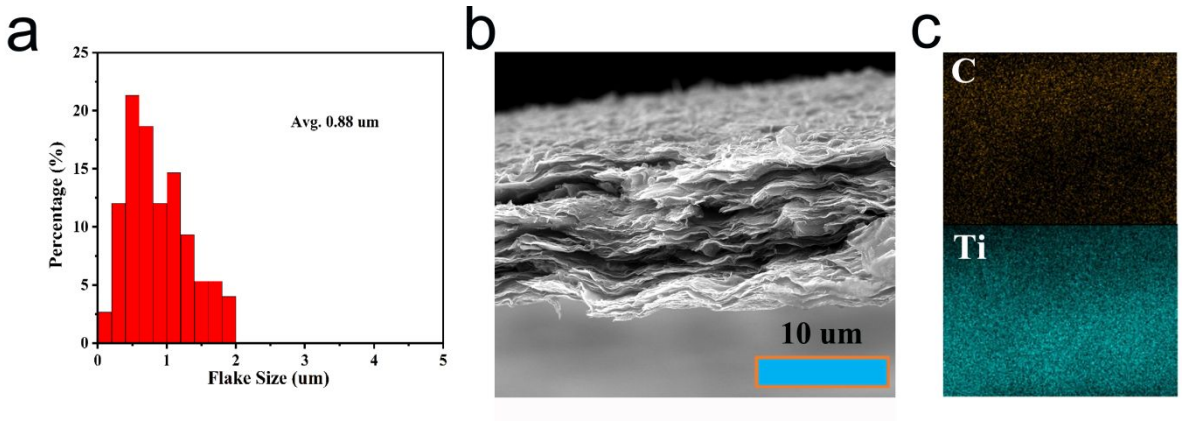

Fig. S2. (a) The flake-size distribution of MXene nanosheets; (b) Cross-section image of the $Ti_3C_2T_x$ film and (c) the corresponding EDS elemental mappings of C and Ti.

Fig. S3

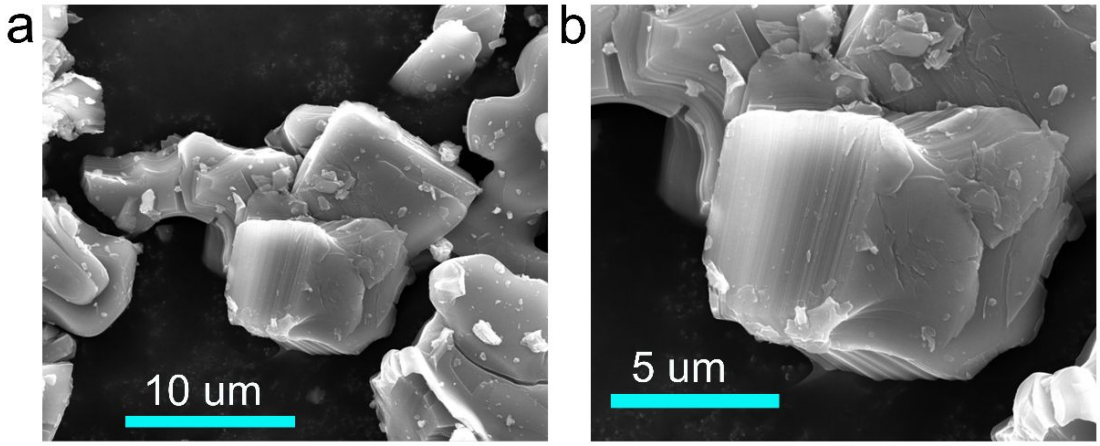

Fig. S3. (a-b) SEM images of the Ti_3AlC_2 nansheets at different magnifications.

Fig. S4

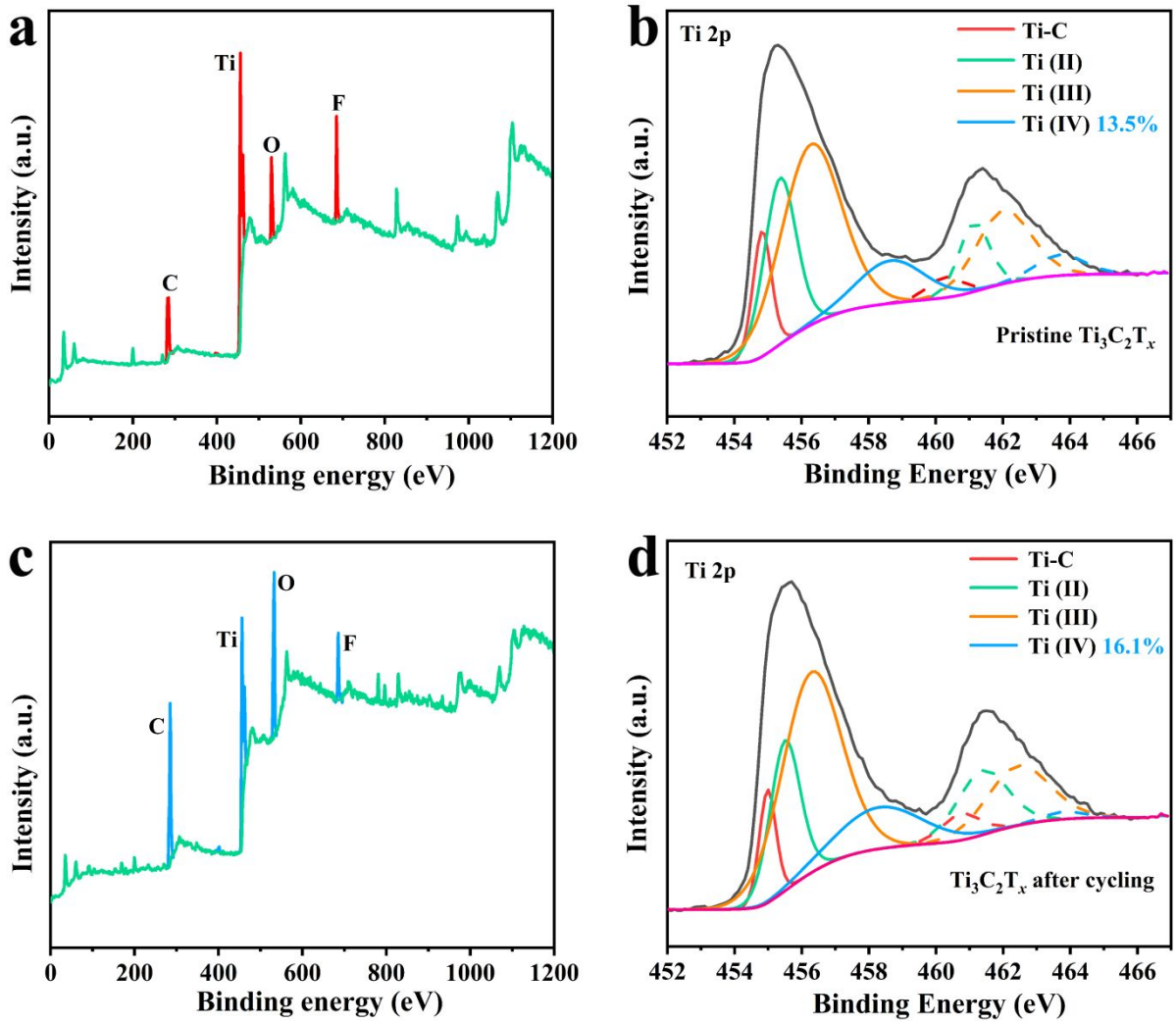

Fig. S4. (a) XPS survey spectrum of the $Ti_3C_2T_x$ film. (b) Ti 2p XPS spectra of the $Ti_3C_2T_x$ film. (c) XPS survey spectrum of the $Ti_3C_2T_x$ film after activation. (d) Ti 2p XPS spectra of the $Ti_3C_2T_x$ film after activation.

Fig. S5

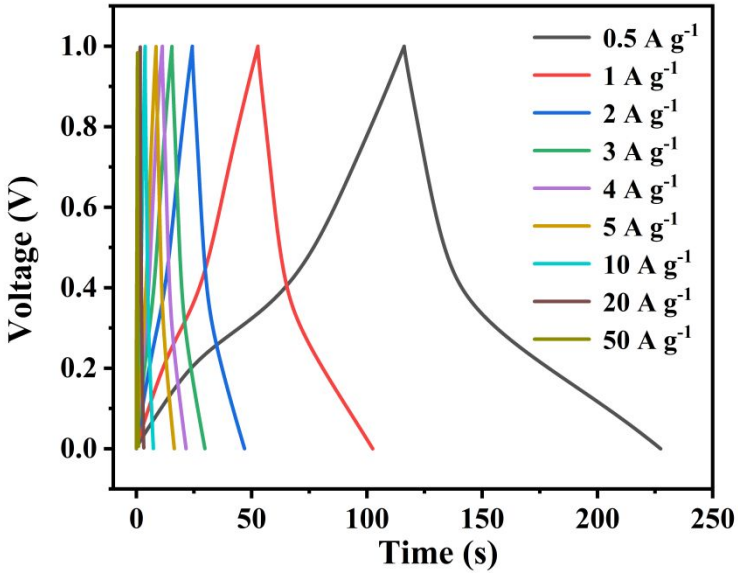

Fig. S5 GCD curves of the $Ti_3C_2T_x$ film based SCs in 3 M H_2SO_4 electrolyte.

Fig. S6

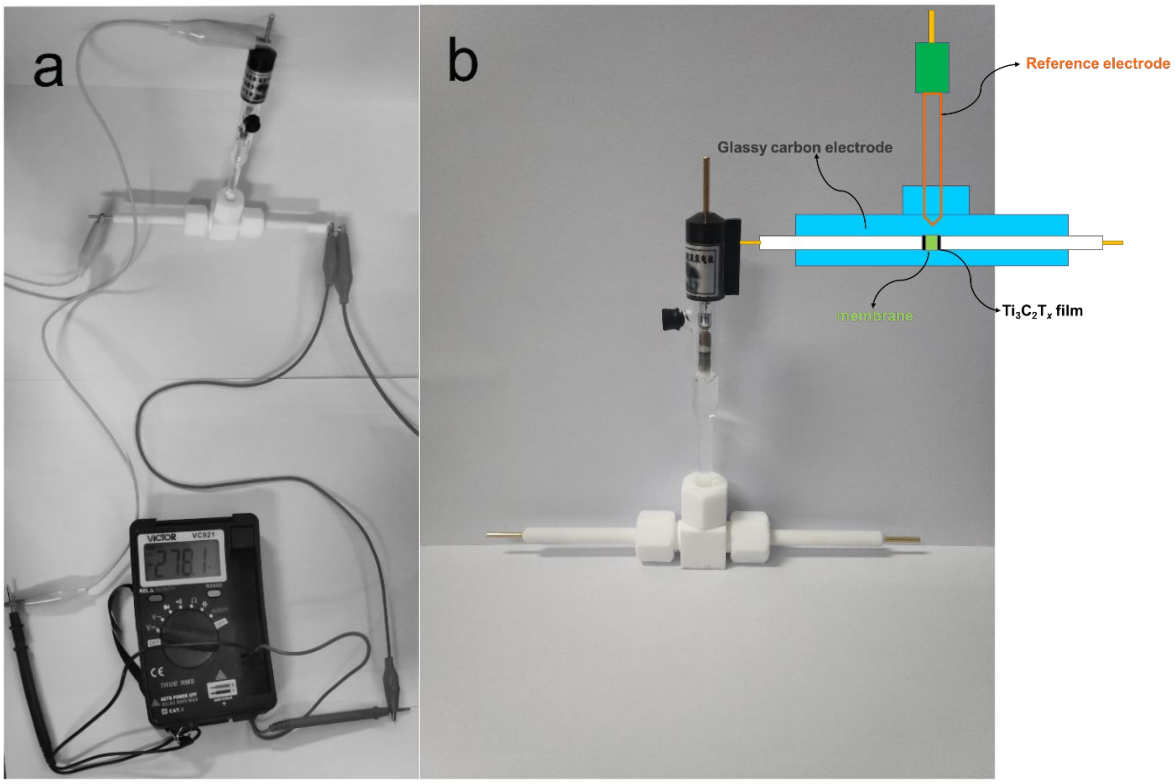

Fig. S6. (a) Device to measure the working potential range of the positive and negative electrodes, (b) Swagelok equipment used to measure the progress characteristics and the schematic diagram of the Swagelok equipment.

Fig. S7

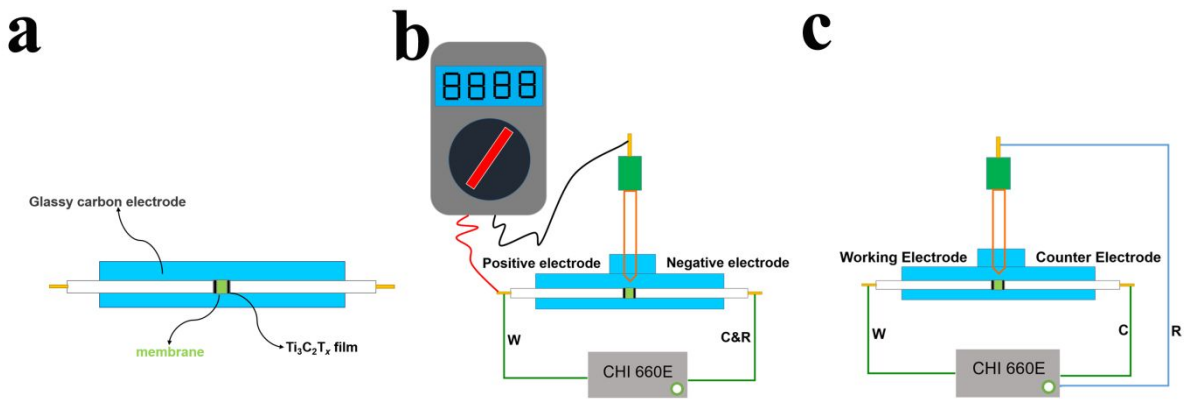

Fig. S7 (a) Standard two-electrode system : The system only can obtain the overall performance of supercapacitors; **(b) Improved two-electrode system:** in this system, the reference electrode is introduced to set up a third circuit to monitor the potential variation of each electrode in the actual working process of supercapacitors; **(c) Three-electrode system:** this method can be used to investigate the real capacitance behavior of electrode materials in the positive and negative potential range, thus avoiding the interaction between the positive and negative electrodes.

Fig. S8

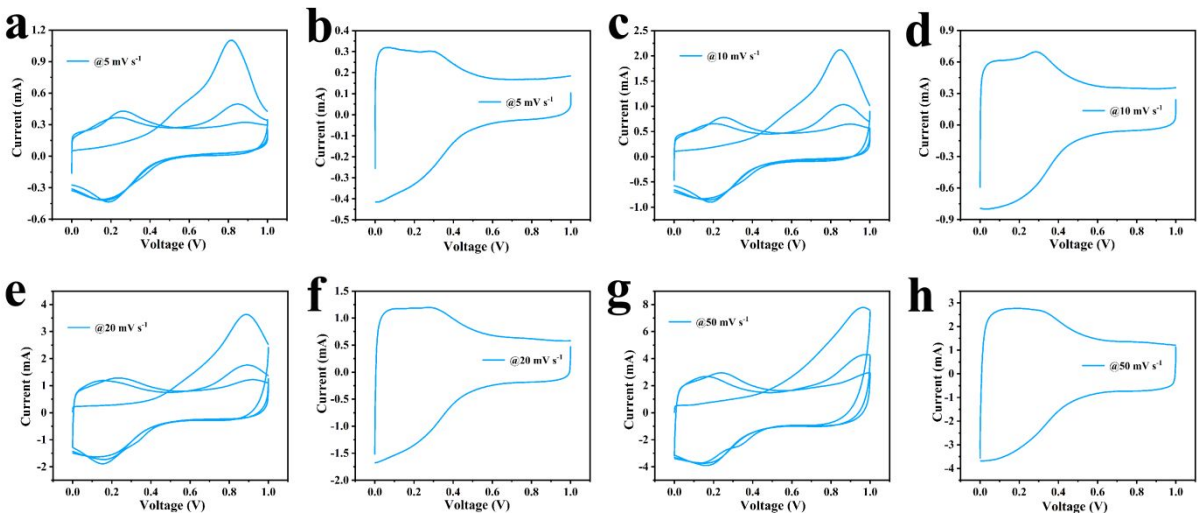

Fig. S8 CV curves of the $Ti_3C_2T_x$ based symmetric SC for the first 3 cycles at different scan rates: (a) 5 mV s^{-1}, (c) 10 mV s^{-1}, (e) 20 mV s^{-1} and (g) 50 mV s^{-1}. CV curves of the $Ti_3C_2T_x$ based symmetric SC after activation at differnt scan rates: (b) 5 mV s^{-1}, (d) 10 mV s^{-1}, (f) 20 mV s^{-1}, and (h) 50 mV s^{-1}.

Fig. S9

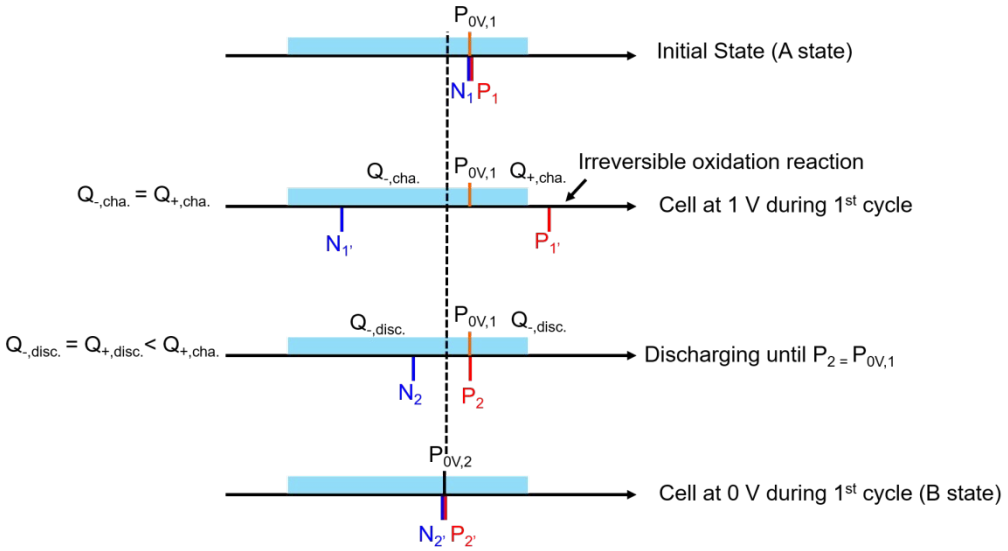

Fig. S9 The blue area is the available potential for Ti_3C_2 MXene in 3 M H_2SO_4 electrolyte; N and P represent the potential of the positive and negative electrodes, respectively.

Fig. S10

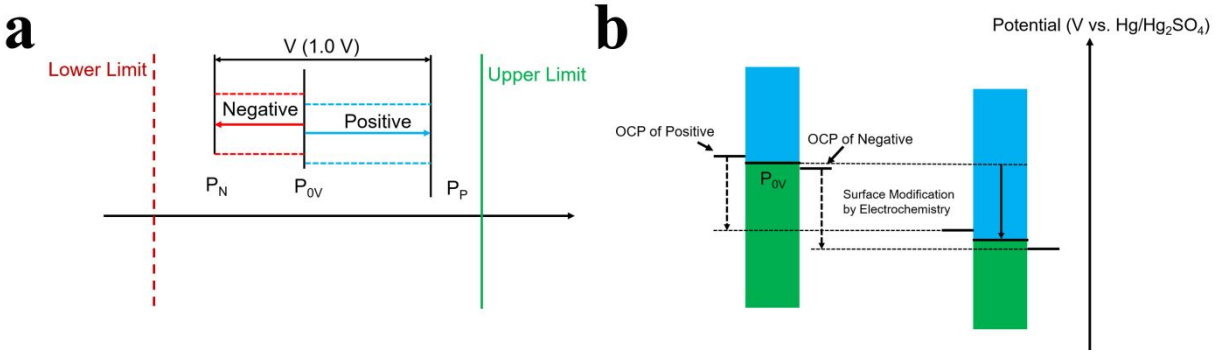

Fig. S10 (a) Parameters: P_N and P_P represent the potential of the negative and positive electrodes, respectively. P_{0V} represents the potential of both electrodes when the SCs are operated at 0 V. **(b)** Illustration of P_{0V} shifting to a lower potential with electrochemical surface modification.

Fig. S11

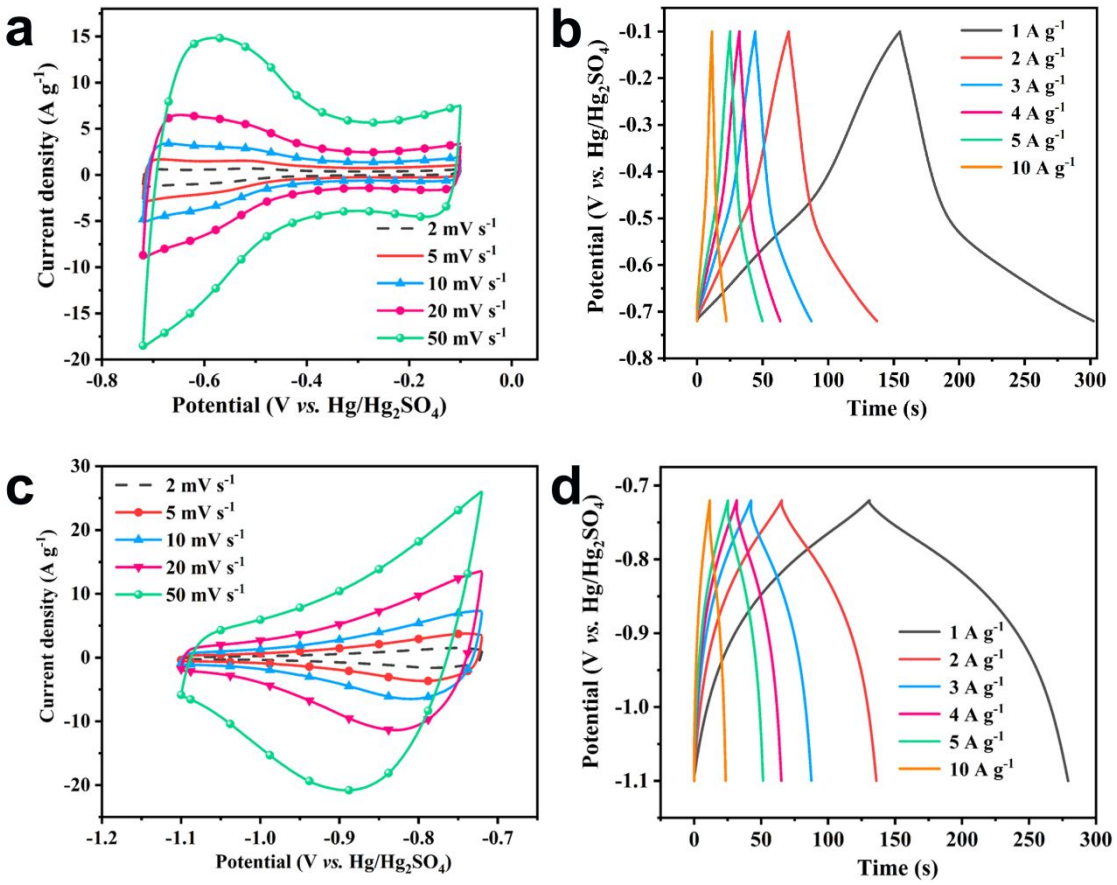

Fig. S11. (a) CV curves of the positive electrode at the scan rates of 2, 5, 10, 20 and 50 mV s^{-1}. (b) GCD curves of the positive electrode at different current densities. (c) CV curves of the negative electrode at the scan rates of 2, 5, 10, 20 and 50 mV s^{-1}. (d) GCD curves of the negative electrode at different current densities. All the data were tested under the condition of three-electrode system.

Fig. S12

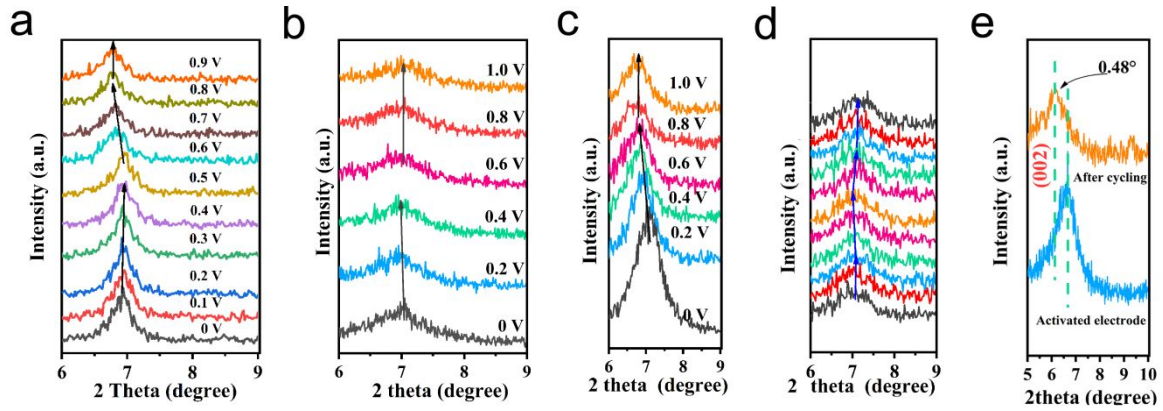

Fig. S12. In situ XRD patterns for the negative electrode (a) and positive electrode in the mixed electrolyte (b), the negative electrode (c) and the positive electrode (d) in the H_2SO_4 electrolyte. (e) The XRD patterns for the positive electrode for the sample of the activated electrode (after 30 cyclings) and the sample after 5000 cycles in the mixed electrolyte.

Fig. S13

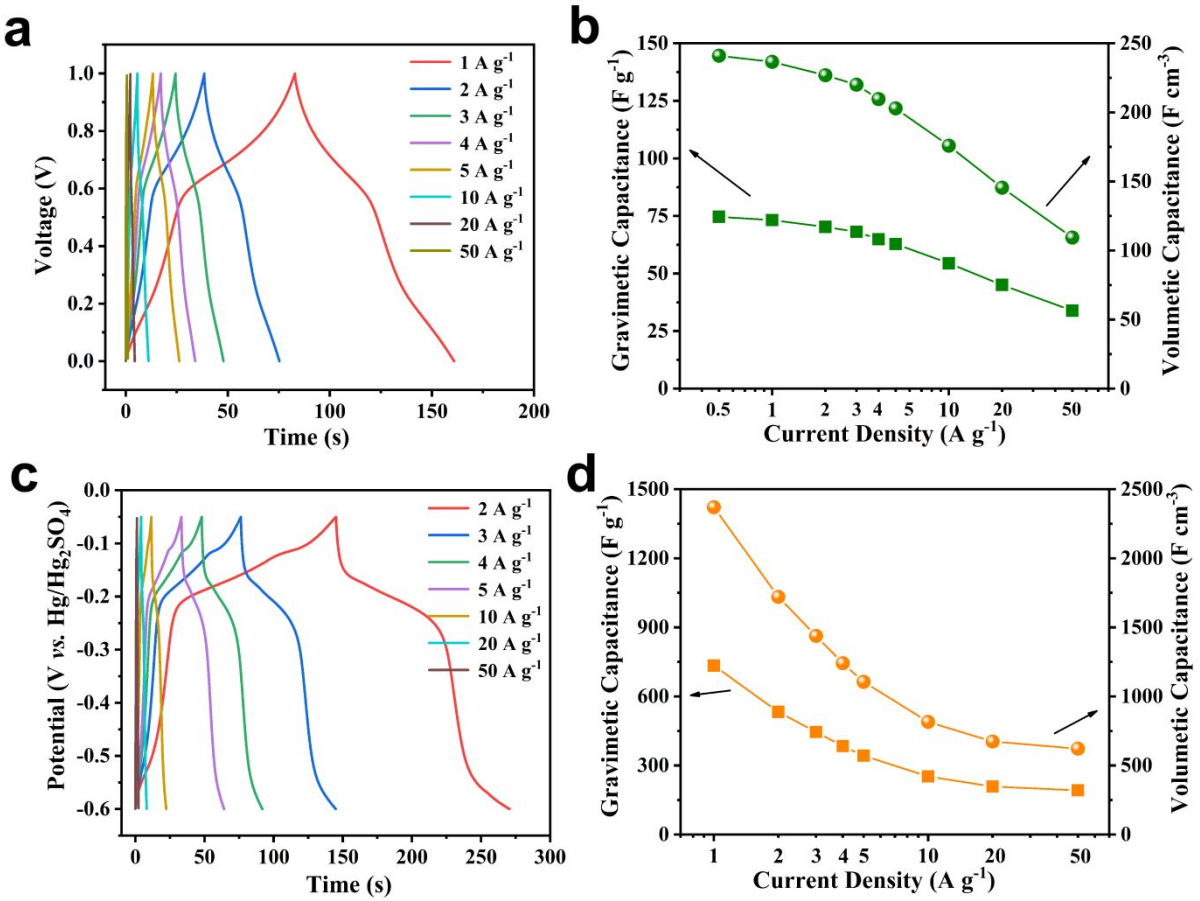

Fig. S13 (a) GCD curves for the cell in the mixed electrolyte at different current densities. (b) Gravimetric capacitance and volumetric capacitance of the cell in the mixed electrolyte calculated from the GCD curves. (c) GCD curves of the MXene electrode in the mixed electrolyte at different current densities in the form of three-electrode system. (d) Gravimetric capacitance and volumetric capacitance of the MXene electrode in the mixed electrolyte in the form of three-electrode system calculated from the GCD curves.

Fig. S14

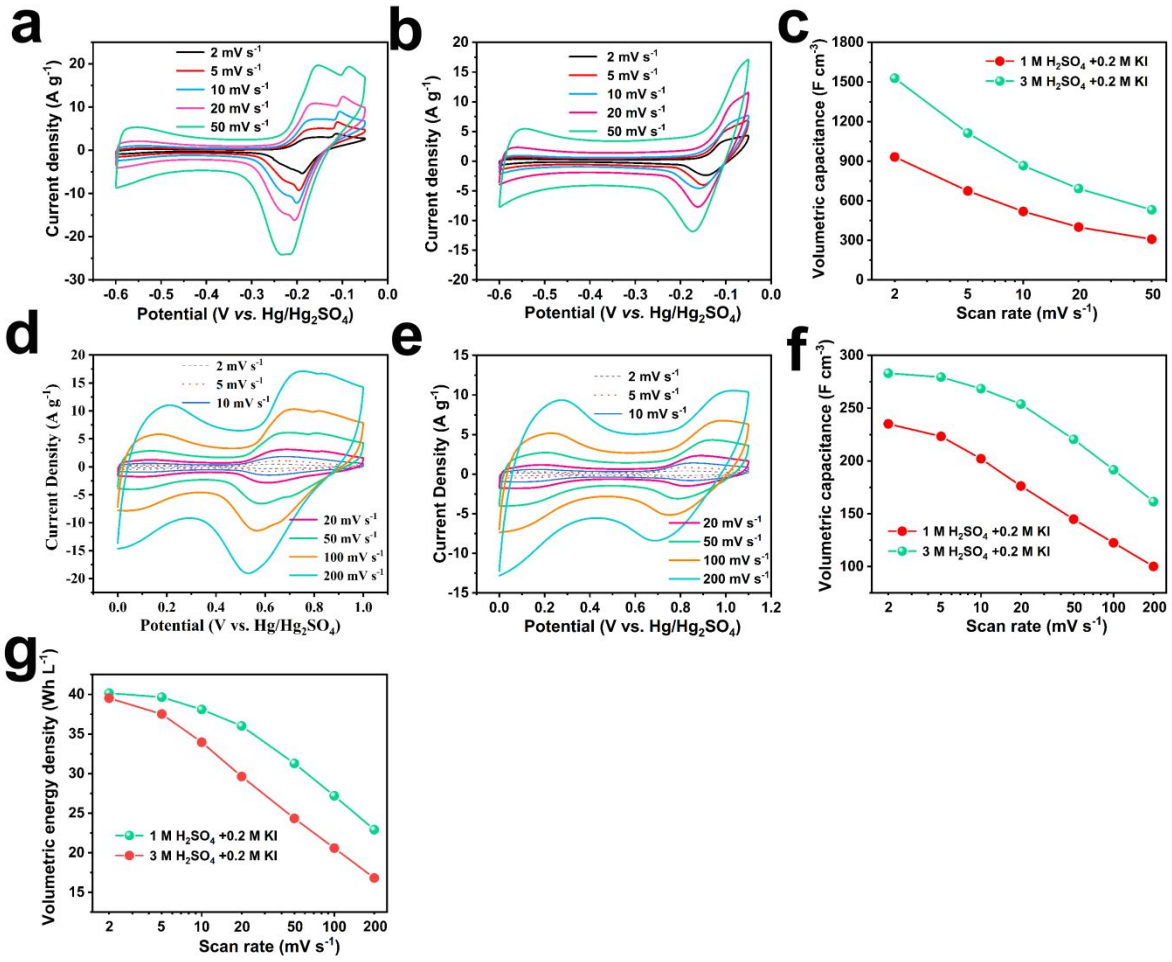

Fig. S14 CV curves for the MXene electrode in 3 M H_2SO_4 + 0.2 M KI (a) and 1 M H_2SO_4 + 0.2 M KI (b) in the form of three-electrode system. (c) Volumetric capacitance of the electrode in different electrolytes at different scan rates calculated from the CV data. CV curves of the MXene based cells in 3 M H_2SO_4 + 0.2 M KI (d) and 1 M H_2SO_4 + 0.2 M KI (e) electrolytes. (f) Volumetric capacitance of the cell in different electrolytes at different scan rates calculated from the CV data. (g) Volumetric energy density of the cell in different electrolytes at different scan rates.

Fig. S15

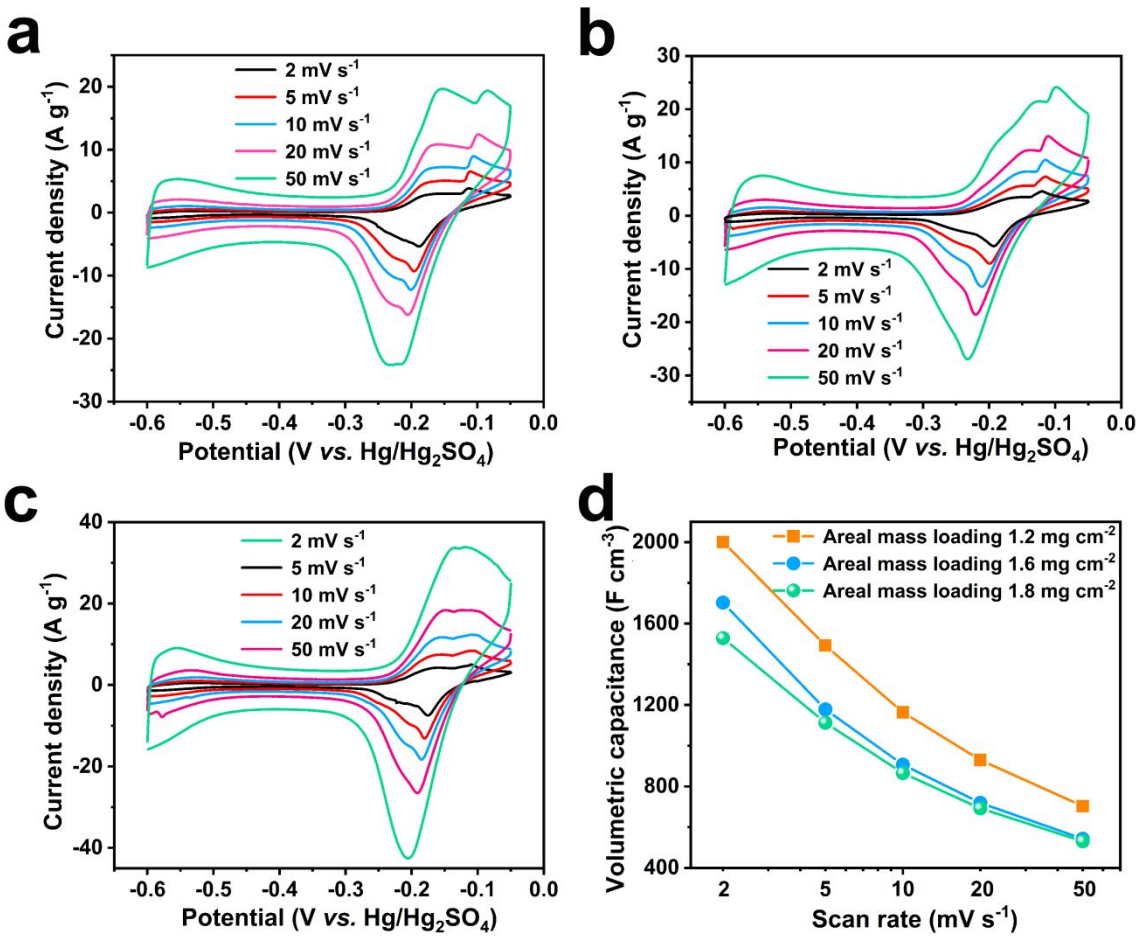

Fig. S15. CV curves of the MXene electrode with different real mass loading in 3 M H_2SO_4 + 0.2 M KI electrolyte under three-electrode system at the scan rates of 2, 5, 10, 20, and 50 mV s^{-1}: (a) 1.8, (b) 1.6 and (c) 1.2 mg cm^{-2}. (d) Volumetric capacitance of the MXene electrode with different real mass loadings at different scan rates.

Fig. S16

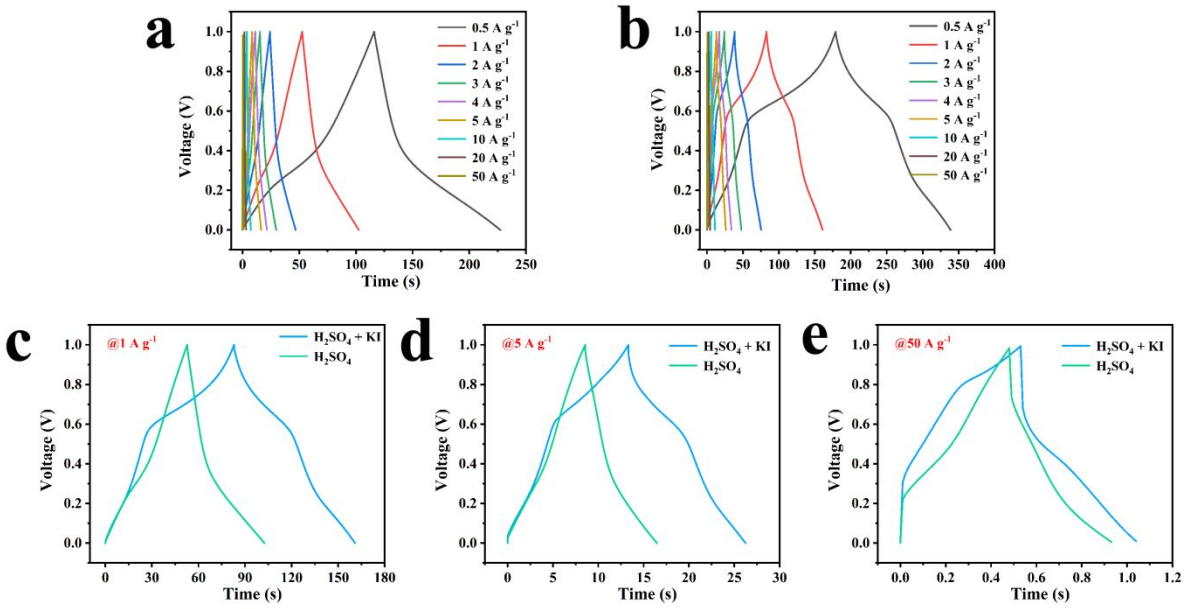

Fig. S16. GCD curves of the $Ti_3C_2T_x$ film based SCs in 3 M H_2SO_4 (a) and 3 M H_2SO_4 + 0.2 M KI electrolytes (b). GCD curves of the $Ti_3C_2T_x$ film based SCs in 3 M H_2SO_4 and 3 M H_2SO_4 + 0.2 M KI electrolytes based on the total mass of the two electrodes at differnt current densities: (c) 1 A g^{-1}, (d) 5 A g^{-1} and (e) 50 A g^{-1}.

Fig. S17

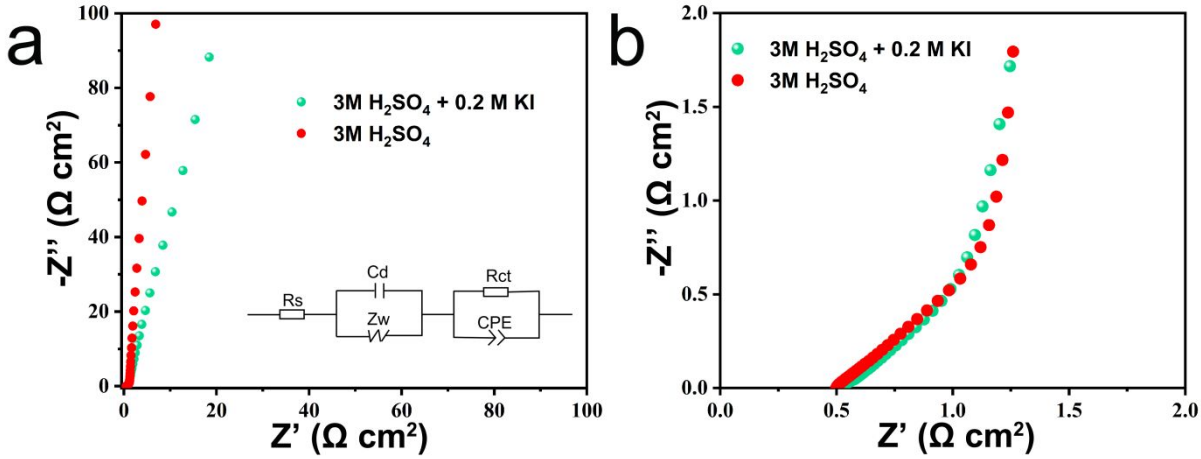

Fig. S17. (a) Nyquist plots of the $Ti_3C_2T_x$ film based cells in 3 M H_2SO_4 and 3 M H_2SO_4 + 0.2 M KI electrolytes and its electrical equivalent circuit. (b) Magnified high-frequency region of the Nyquist plots.

The internal resistance (Rs) is 0.50 and 0.52 Ω cm^2 for the cell in 3 M H_2SO_4 and 3 M H_2SO_4 + 0.2 M KI electrolytes, which prove that the introduction of KI almost has no effect on Rs. At the same time, the charge transfer resistance (Rct) is 1.0 and 1.6 Ω cm^2 for the cell in 3 M H_2SO_4 and 3 M H_2SO_4 + 0.2 M KI electrolytes, in which the higher Rct is absorbed to the charge transfer progress of I^-/I_3^-.